Noname manuscript No.
(will be inserted by the editor)

On Gaseous Emissions during Alumina Feeding

Sindre Engzelius Gylver · Åste Hegglid Follo · Vegard Aulie · Helene Marie Granlund · Anders Sørhuus · Espen Sandnes · Kristian Etienne Einarsrud

Abstract Aluminium electrolysis involves feeding of alumina into a cryolite based bath. Water originating from alumina as well from air reacts with fluorides and results in HF evolution. Untreated HF gas is a significant environmental and economical issue. HF is however effectively adsorbed in (primary) alumina before being fed back to the cell as secondary alumina, thereby recycling the fluoride. As alumina is fed to the cell, it forms a raft, delaying the dissolution process and linked to several operational challenges.

The goal of the current work is twofold; first, water content is investigated in a lab scale setting, aiming to explain raft porosity, ultimately causing it

Sindre Engzelius Gylver
Department of Material Science and Engineering, NTNU, Trondheim, Norway
Tel.: +47 48252061
E-mail: sindre.e.gylver@ntnu.no

Åste Hegglid Follo
Department of Material Science and Engineering, NTNU, Trondheim, Norway
E-mail: aste.hegglid.follo@elkem.no

Vegard Aulie
Department of Material Science and Engineering, NTNU, Trondheim, Norway
E-mail: vegaraul@stud.ntnu.no

Helene Marie Granlund
Alcoa Norway Ans, Mosjøen, Norway
E-mail: Helene.Marie.Eng.Granlund@alcoa.com

Anders Sørhuus
GE Power Norway AS, Oslo, Norway
E-mail: anders.sorhuus@ge.com

Espen Sandnes
Department of Material Science and Engineering, NTNU, Trondheim, Norway
E-mail: espen.sandnes@ntnu.no

Kristian Etienne Einarsrud
Department of Material Science and Engineering, NTNU, Trondheim, Norway
Tel.: +47 97007236
E-mail: kristian.e.einarsrud@ntnu.no

to float rather than disperse in the bath. Secondly, the evolution of HF is investigated for different aluminas in both a lab scale setting and in industrial measurements performed at Alcoa Mosjøen, aiming to identify correlations between gas evolution and alumina properties.

Keywords Alumina feeding · Rafts · HF Emissions

1 Introduction

Besides being the principal raw material, alumina plays an important role as a cleansing agent in modern smelters. By the dry scrubbing process, toxic hydrogen fluoride gas is adsorbed onto fresh alumina, creating what is known as secondary alumina. Other benefits include the recycling of fluorides back to the cell and better dissolution of alumina [1].

HF is generated when water reacts with fluorides present in the bath, either to entrained bath:

$$\frac{2}{3}AlF_3(diss) + H_2O(g) = 2HF(g) + \frac{1}{3}Al_2O_3(diss) \tag{1}$$

or by hydrolysis of pot fume [2]

$$NaAlF_4(g) + H_2O(g) = 2HF(g) + \frac{1}{3}Al_2O_3(s) + \frac{1}{3}Na_3AlF_6(s) \tag{2}$$

The source of water is mainly from moisture present in the alumina, although hydrogen in the anodes as well as ambient moisture is also of importance. Hyland et al. [3] point out that hydrogen incorporated into the crystal lattice, also known as structural hydroxides, contributes significantly to the formation of HF. These groups are often measured as LOI 350-1000, and will be released slowly as alumina is dissolved and results in a slower and more continuous release of HF gas, compared to more loosely bound water.

Alumina is added in batches through point feeders, where about 1 kg of powder is added at each feeding. Upon a addition, a rigid structure known as a raft, floating on the bath surface, might be formed. Rafts from industrial cells have been collected and characterized in earlier work, revealing a porous structure as well as large cavities [4]. Rolseth and Thonstad [5] created crusts by adding alumina to bath in a lab scale furnace, revealing that the crusts created from secondary alumina have a more porous structure than from primary [6]. The source of the pores are however not thoroughly investigated yet, but it is believed to be related to the release of moisture and hydroxyl groups or impurities such as sulfur [7] or fluorides [8] forming gaseous species such as SO_2 and HF, which gets trapped as the bath solidifies.

Measurements of HF has been done in several smelters. Previous measurements suggest that the HF content is about 200-400 ppm in the duct, and is dependent of cell technology [9–11]. The evolution of HF has been found to be closely related with the feeding cycle, where a peak in HF content is

registered short time after alumina is added, explained by the moisture contribution from alumina. A rise in the HF concentration is also observed when the cell is overfeeding.

Previous industrial data suggest that the condition of feeding hole and crust has a major effect on the measured HF content. By creating a portable probe connected to a Tuneable Diode Laser (TDL), Osen et al. [12] were able to measure the HF content at several position in an industrial cell. They measured HF content up to 9000 ppm in the feeding hole, while the content above the crust far away from the feeding hole were 5-10 ppm. Slaugnehapt et al. [9] covered the feeding holes while monitoring the HF evolution from the off gas. They observed that the effect of a closed feeding hole were much larger than low bath ratio and high temperature, which will increase the vapor pressure of the bath.

The effect on routine operations are also observed, in particular by Patterson [11]. During anode change, high values of HF were measured, which was explained by a large surface of bath is available as the anode is removed. Metal tapping was also observed to increase HF evolution, and is explained by change in crust integrity due to anode movement after tapping. Increased humidity has also been observed to affect the measured content, due to more available water in the atmosphere.

The current work aims to extend the existing body of knowledge related to HF evolution during alumina feeding. Dedicated lab scale experiments are performed in order to study the link between moisture, HF evolution and raft porosity, while industrial measurements have been carried out over 43 consecutive days in order to investigate the influence of cell operations and conditions of HF evolution.

2 Experimental details

2.1 Formation of rafts

The lab scale experiments were performed with industrial bath with properties as given in Table 1. Primary and secondary alumina from the industry was used for the experiments, with particle size distribution given in Table 1. Since the main goal of the current work is to study the effect of water content, other parameters, such as flouride and α-content, are not quantified in this study. Different water content was achieved by either drying or hydrating the powder, summarized as LOI Room Temperature (RT)-1000 in Table 1 for primary and secondary alumina. The LOI values used in the current work are considerably higher than that expected in an industrial setting, but were used in order to more easily observe any trends.

The set-up and method for generating and extracting rafts was based on the work of Gylver et al. [13], as sketched in Figure 1. A carbon crucible was filled with 1300 g of industrial bath, corresponding to a molten bath height of 6.5 cm, and placed in a furnace with inner diameter of 15 cm and

Table 1 Physical data of the bath and particle distribution for the alumina types.

Bath Properties	Value
Bath acidity	10.8 wt%
Alumina content at start	2.3 wt %
Primary Alumina Properties	**Value**
+ 149 μm	1.1 %
- 44 μm	9.8 %
- 20 μm	1.2 %
LOI RT-1000 Dry	2.81 %
LOI RT-1000 Medium	4.29 %
LOI RT-1000 Hydrated	5.67 %
Secondary Alumina Properties	**Value**
+ 149 μm	3.2 %
- 44 μm	7.7 %
- 20 μm	0.5 %
LOI RT-1000 Dry	3.57 %
LOI RT-1000 Medium	5.02 %
LOI RT-1000 Hydrated	6.37 %

41 cm height. The furnace was purged with 99.999 % pure Nitrogen gas in order to decrease air burn on the carbon crucible. Temperature was monitored throughout the experiments using a S-type thermocouple placed inside a steel tube at the periphery of the crucible, immersed about 4 cm into the bath. In order to prevent heat loss during the experiment, the furnace was covered during addition and formation of rafts, thus preventing visual observations.

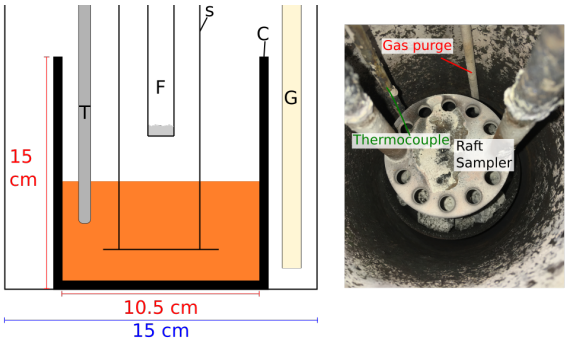

Fig. 1 Left: Vertical cross section of the furnace, equipped with thermocouple (T), feeding pipe (F), raft sampler (S), carbon crucible (C) and gas purge (G). Right: Image of the furnace seen from above.

Alumina feeding was done through a 50 cm long pipe with an inner diameter of 1 cm, equipped with a bottom mounted lid, which was actuated by a spring button on the top of the pipe, placed such that alumina was released 2 cm above the bath surface. 4 grams of alumina was added to the bath, and the created raft was removed from the bath after 60 seconds and cooled under ambient conditions. A total of 18 rafts were created.

After extraction, the rafts were weighed and photographed and their structure was analyzed using Micro computed X-ray tomography (μCT). The data was acquired using a Nikon XT H225 ST instrument (cone beam volume CT), using a tungsten reflection target and an aluminum filter of 1 mm, with an acceleration voltage of 140 kV and a current of 150 μA. The imaging was done with an integration time of 1 s, amplification of 18 dB, with 3142 projections per 360°. Images obtained by μCT were further processed in ImageJ [14] in order to determine raft porosity.

2.2 Industrial HF-measurements

A Neo Monitors Lasergas™ II SP was installed in the off-gas channel, 15 meters away from the cell at the Alcoa Mosjøen plant. The TDL monitored the HF content all day long,in the period July 4th to August 15th 2019, with measurement intervals varying between 1 and 10 seconds, which was adjusted manually.

The temperature was measured with STARprobe™ [15] every second day as a part of routine operations. As a part of the campaign, a higher voltage was applied to the cell for one day, in order to obtain a higher bath temperature. Measurements with STARprobe™ were conducted six times on this day with approximately 2 hours between each measurement.

3 Results and discussion

3.1 Lab scale rafts

Sample CT images of rafts created from primary and secondary alumina are shown in Figure 2, while Figure 3 shows the calculated porosity for all collected samples. The porosity is reported as the amount of (closed) pores relative to the entire horizontal cross sectional area of the sample. The (closed) pores are actual voids in the raft, which otherwise consists of alumina particles in a bath matrix [4].

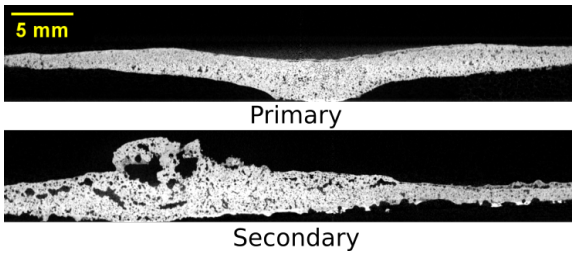

Fig. 2 CT images of rafts created from primary (top) and secondary (bottom) alumina.

The porosity is due to both small pores and larger cavities, also observed in earlier work, and is found to be more important for the rafts created from

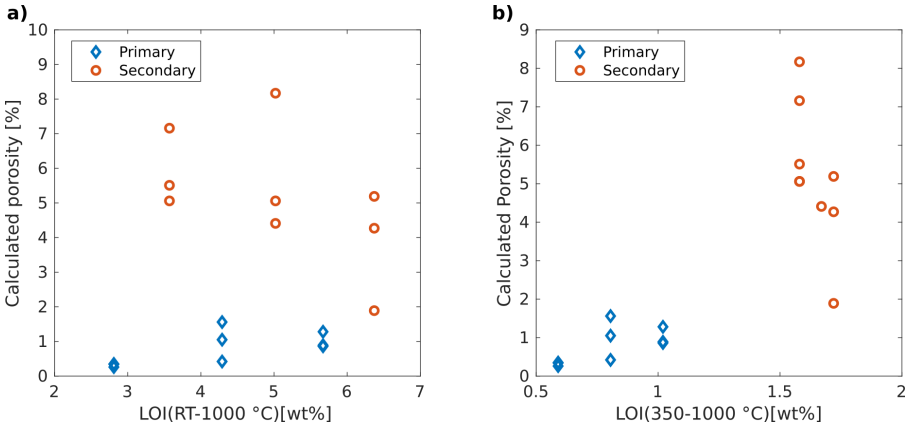

Fig. 3 The calculated porosity for rafts created from primary(diamonds) and secondary(circles) alumina, with different water content - represented as LOI RT-1000 a) and LOI 350-1000 b).

secondary alumina. Rafts generated from secondary alumina typically had a large cavity in the central regions (see lower image in Figure 2), while those generated from primary where typically thin and disk-like. Considering Figure 3a, there is no apparent link between the porosity and LOI RT-1000. This is believed to be due to excess water on the surface flashing off immediately after addition. Results for LOI 350-1000, Figure 3b, however indicate that higher values of this parameter are linked to greater porosities. The LOI 350-1000 interval will account for release of both structural water and fluoride impurities [8] present in the (secondary) alumina, thus indicating that the pores at least in part can be explained by HF gas which becomes trapped in the raft as it is formed.

3.2 Industrial measurements

Figure 4 demonstrates the measured HF content under normal operations. Each feeding event (red dots in sub-figures b,c,d) is typically followed by a peak in HF, which then drops off more slowly. The peaks are typically registered about 30 seconds after feeding. An examination of data during high measurement frequency was calculated to be 31.73 ± 0.24 s. Corresponding delays between feeding events and peak values have been observed in earlier measurements within the same cell technology [10]. Several factors are believed to contribute to this delay, relating to HF gas formation and subsequent transport from the bath and into the duct where concentrations are measured. Under normal conditions, this transport will take place through the feeding hole. If the feeding hole is closed, the time for the HF to arrive in the duct will increase, which can explain some of the variation seen in our measurements.

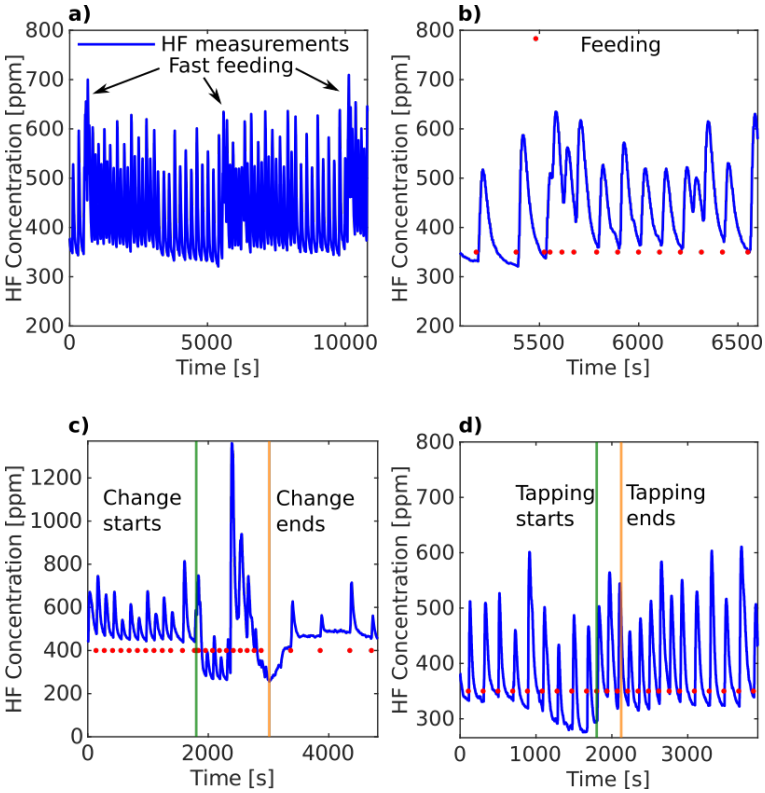

Fig. 4 Measurements of HF during normal operations. a): Typical measurement of HF content during three hours. b) A section of the measurement from a), where fast feeding occurs. Feedings are indicated with red dots. c) Measurement during anode change. d) Measurement during tapping.

As seen in Figure 4, the increase in HF content is rapid, while it declines more slowly. While this behavior is the expected response from a ideal reactor experiencing a pulse - e.g. feeding - the decline may also be related to delayed gas release arising due to bath freezing around the added alumina, forming a raft, as readily observed in the same cell design [16] previously. Gas may also be trapped within the porous structure of the raft, as observed both under lab-scale conditions, as in the current work, as well as in industry [4].

The data presented in Figure 4 indicates the presence of two time-scales, one being the time between each subsequent feeding event, denoted as t_f and one related to the (typical) length of the feeding cycle, t_c. In order to quantify the impact of the various cell operations and conditions, mean and extremal quantities are calculated for each of the time scales considered. Denoting the measured HF concentration by $C(t)$, the time averaged concentration between

two feeding events, $\bar{C}_{fa}$ and over a given feeding cycle $\bar{C}_{ca}$ is given as

$$\bar{C}_{fa} = \frac{1}{t_f} \int_{t_f} C(t)dt \tag{3}$$

$$\bar{C}_{ca} = \frac{1}{t_c} \int_{t_c} C(t)dt \tag{4}$$

The base values for a single feeding event C_{fb} and the full cycle, C_{cb} are defined as:

$$C_{fb} = min\,|C(t)|_{t_f} \tag{5}$$

$$C_{cb} = mean(C_{fb})|_{t_c}, \tag{6}$$

where min_{t_f} and $mean(C)|_{t_c}$ signify the minimum and arithmetic values over the time interval in question. Correspondingly, the peak values C_{fp} and C_{cp}, are calculated as

$$C_{fp} = max|C(t)|_{t_f} \tag{7}$$

$$C_{cp} = mean(C_{fp})|_{t_c}. \tag{8}$$

Finally, the peak-to-peak values are defined as

$$C_{f,P2P} = C_{fp} - C_{fb} \tag{9}$$

and

$$C_{c,P2P} = C_{cp} - C_{cb}. \tag{10}$$

Statistics for all calculated parameters are presented in Table 2. Evidently, there is considerable deviation in the data set, in particular for the quantities defined for the feedings.

Table 2 Mean and standard deviation for the concentration values described by equations (3)-(10) for the entire campaign.

Quantity	Mean [ppm]	Standard deviation
$\bar{C}_{fa}$	424.14	80.70
$\bar{C}_{ca}$	413.82	54.14
C_{fb}	332.33	63.44
C_{cb}	334.16	47.40
C_{fp}	581.31	97.89
C_{cp}	583.69	66.68
$C_{f,P2P}$	248.98	76.78
$C_{c,P2P}$	249.53	43.70

From the raw data presented in Figure 4, there appears to be some trends with respect to feed-values C_{fi} (i.e. equations 3, 5, 7 and 9), following changes in the feeding cycle, tapping and anode change, which can explain some of the variation observed in Table 2. These possible trends are investigated further and quantified in the following paragraphs.

Considering changes in the feeding cycle, a total of 711 cycles were investigated. Within each cycle j, a linear regression model was made for each of the variables C_{fi}:

$$C(t)_{fi} = b_i - a_i t, \quad t \in t_c^j, \tag{11}$$

as illustrated in Figure 5.

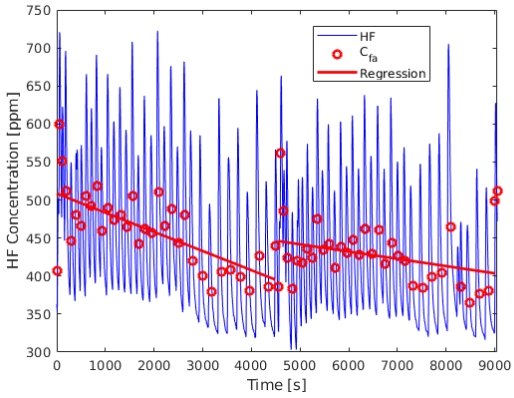

Fig. 5 Two feeding cycles where $\bar{C}_{fa}$ and its estimated regression lines are shown.

The slopes a_i were assumed to be normal distributed and a t-test with the null hypothesis $a = 0$ vs $a > 0$ was performed in order to determine any significant trends, with main results presented in Table 3. As shown in the table, both $\bar{C}_{fa}$ and C_{fb} meet the hypothesis, while C_{fp} and $C_{f,P2P}$ do not. These results indicate that the HF-emissions are lower as the cell is underfed, since less alumina and hence surplus fluoride is entering the cell.

Table 3 Results from one-sided hypothesis test

Quantity	$\bar{a}_i$	Lower limit
$\bar{C}_{fa}$	0.027	0.022
C_{fb}	0.021	0.017
C_{fp}	0.0037	-0.0078
$C_{f,P2P}$	-0.0175	-0.028

For tapping and anode change, average C_{fi} values were calculated for the 10 feedings before and the 10 first feedings after the operation. For the anode change operation, these averages $\tilde{C}_{fa}$ are shown in Figure 6. A hypothesis test shows that the HF concentration after anode change is significantly lower after anode change than before. It should however be noted that alumina is fed at a lower frequency following anode change (cf. Figure 4) and it is therefore challenging to distinguish if the anode change itself affects the emissions or if the observation is due to the altered feeding conditions.

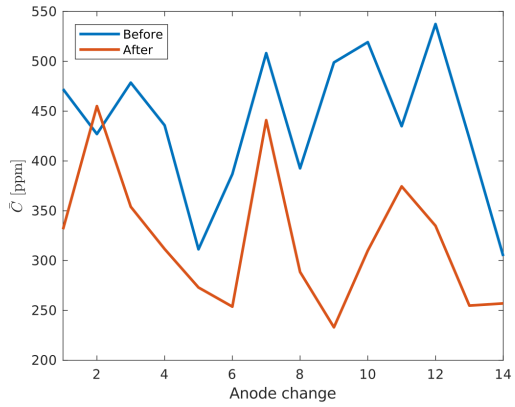

Fig. 6 $\bar{C}_1$ calculated for 10 feedings right before/after anode change, where 14 different anode changes are considered.

The same procedure was used to investigate the tapping process, but no significant difference was found for this operation.

For temperature, average properties were calculated based on five feeding events before and after the temperature was measured, as shown in Figure 7. The current data indicates a significant positive correlation between temperature and HF emissions, which is in accordance with earlier research [2].

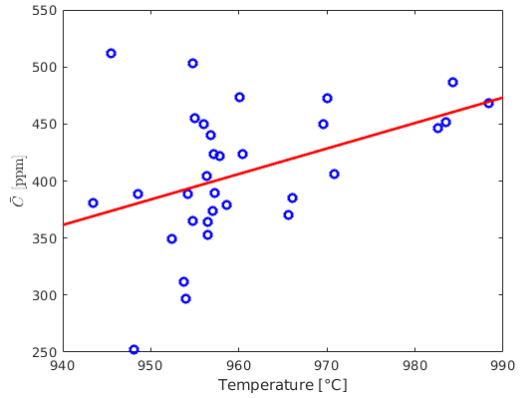

Fig. 7 Temperatures and $\bar{C}$, where $\bar{C}$ is calculated as a mean from 5 feedings before and 5 feedings after the temperature was measured.

Finally, HF measurements were compared to the absolute humidity in proximity of the smelter [17]. A representative example showing humidity and measured HF concentration over three days is shown in Figure 8. There is considerable variation both humidity and HF emissions. However, the Pearson correlation coefficient between these two parameters was calculated to be 0.30, indicating no significant correlation in the current campaign.

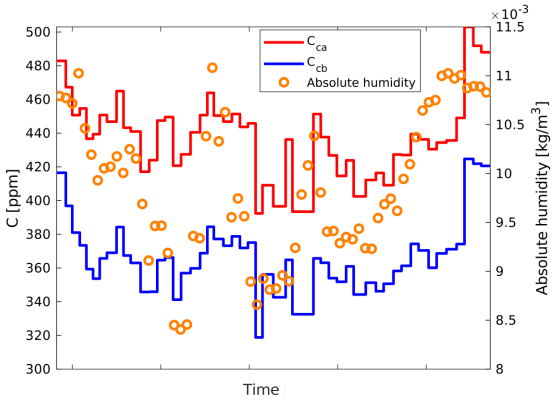

Fig. 8 The calculated values of $\bar{C}_{ca}$ and C_{cb} together with relative humidity plotted over 3 consecutive days.

4 Conclusions

Alumina feeding and HF evolution is investigated on both lab- and industrial scale.

Lab scale measurements show that there is a significant difference in porosity between rafts generated from primary and secondary alumina. The difference appears to be related to LOI 350-1000, i.e. structural hydroxides and fluoride impurities, indicating that the porous structures observed are due to HF evolution. While the porous structures are believed to contribute significantly to the buoyancy of the rafts and thereby delay dissolution, several other alumina properties will affect the dissolution as well. These factors will be investigated in future work.

Industrial scale measurements have been performed over 43 consecutive days, aiming to investigate possible correlations between HF emissions and cell operations and conditions. On average, the HF concentration was measured to be around 400 ppm in the duct during the campaign.

A rapid rise in measured HF is observed after each feeding, followed by a slower decline. If the rate of decline is dependent on the raft floating time was beyond the scope of this work, but will be looked into in the future.

The feeding cycle appears to play a significant role on the measured HF content. As the the cell is underfeeding, the measured HF concentration is also being reduced. Of regular operations, anode change seems to have a significant role, although this could be masked by changes in the feeding cycle. Tapping does not appear to play a significant role. A correlation between bath temperature and HF content was found, while no correlation between HF content and humidity was identified.

Acknowledgements The current work has been funded by SFI Metal Production (Centre for Research-based Innovation, 237738). The authors gratefully acknowledge the financial support from the Research Council of Norway and partners of the center.

References

1. K. Grjotheim and H. Kvande, Eds., *Introduction to Aluminium Electrolysis-Understanding the Hall-Heroult Process*. Düsseldorf: Aluminium-Verlag, 1993.
2. W. Haupin and H. Kvande, "Mathematical Model of Fluoride Evolution from Hall-Héroult Cells," in *Essential Readings in Light Metals: Volume 2 Aluminum Reduction Technology*, G. Bearne, M. Dupuis, and G. Tarcy, Eds. Cham: Springer International Publishing, 2016, pp. 903–909.
3. M. Hyland, E. Patterson, and B. Welch, "Alumina Structural Hydroxyl as a Continous Source of HF," in *Essential Readings in Light Metals: Volume 2 Aluminum Reduction Technology*, G. Bearne, M. Dupuis, and G. Tarcy, Eds. Cham: Springer International Publishing, 2016, pp. 936–941.
4. S. E. Gylver et al., "The Micro- and Macrostructure of Alumina Rafts," in Light Metals 2019, 2019, pp. 689–696.
5. S. Rolseth and J. Thonstad, "Agglomeration and dissolution of alumina in cryolite baths," in *Extraction, Refining, and Fabrication of Light Metals*, Amsterdam, 1991, pp. 177–190.
6. Y. Yang, B. Gao, Z. Wang, Z. Shi, and X. Hu, "The Formation and Dissolution of Crust Upon Alumina Addition into Cryolite Electrolyte," *Journal of Metals*, vol. 67, no. 9, pp. 2170–2180, Sep. 2015.
7. R. Meirbekova, G. M. Haarberg, J. Thonstad, and G. Saevarsdottir, "Influence of Sulfur Species on Current Efficiency in the Aluminum Smelting Process," *Metall and Materi Trans B*, vol. 47, no. 2, pp. 1309–1314, Apr. 2016.
8. A. R. Gillespie, M. M. Hyland, and J. B. Metson, "The Surface Chemistry of Secondary Alumina from the Dry Scrubbing Process," in *Essential Readings in Light Metals: Volume 2 Aluminum Reduction Technology*, G. Bearne, M. Dupuis, and G. Tarcy, Eds. Cham: Springer International Publishing, 2016, pp. 956–961.
9. M. L. Slaugenhaupt, J. N. Bruggeman, G. P. Tarcy, and N. R. Dando, "Effect of Open Holes in the Crust on Gaseous Fluoride Evolution from Pots," in *Essential Readings in Light Metals: Volume 2 Aluminum Reduction Technology*, G. Bearne, M. Dupuis, and G. Tarcy, Eds. Cham: Springer International Publishing, 2016, pp. 930–935.
10. C. Sommerseth et al., "Correlation between Moisture and HF Formation in the Aluminium Process," in *Light Metals 2011*, S. J. Lindsay, Ed. Cham: Springer International Publishing, 2011, pp. 339–344.
11. E. C. Patterson, "Fluoride emissions from aluminium electrolysis cells," PhD Thesis, The University of Auckland, Auckland, 2002.
12. K. S. Osen, T. A. Aarhaug, A. Solheim, E. Skybakmoen, and C. Sommerseth, "HF Measurements Inside an Aluminium Electrolysis Cell," in *Light Metals 2011*, S. J. Lindsay, Ed. Cham: Springer International Publishing, 2011, pp. 263–268.
13. S. E. Gylver, A. Solheim, H. Gudbrandsen, Å. H. Follo, and K. E. Einarsrud, "Lab Scale Experiments on Alumina Raft Formation," in *Light Metals 2020*, Cham, 2020, pp. 659–663.
14. W. S. Rasband, *ImageJ*. Bethesda, Maryland, USA: U. S. National Institutes of Health, 1997, https://imagej.nih.gov/ij/.
15. X. Wang, B. Hosler, and G. Tarcy, "Alcoa STARprobe^{TM}," in Light Metals 2011, S. J. Lindsay, Ed. Cham: Springer International Publishing, 2016, pp. 483–489.
16. S. E. Gylver, N. H. Omdahl, A. K. Prytz, A. J. Meyer, L. P. Lossius, and K. E. Einarsrud, "Alumina Feeding and Raft Formation: Raft Collection and Process Parameters," in Light Metals 2019, 2019, pp. 659–666.
17. "Norsk Klimaservicesenter." https://seklima.met.no/observations/ (accessed Aug. 09, 2020).